Southern African Large Telescope

RSS Observer's Guide

Eric B. Burgh
Kenneth Nordsieck
University of Wisconsin

Document Number: SALT-3170AM0007

Version 0.5
23 Jan, 2009

Change History

Rev	Date	Description
0.3	July 11, 2005	Updated FP information
0.4	July 21, 2005	Added FP filter list
0.5	Jan 23, 2009	Assigned document #; Converted to non-html/ pdf

Table of Contents

1 Introduction

1.1 The Southern African Large Telescope

SALT Coordinates		
Lat: -32 22 46	Long: 20 48 38.5 E	El: 1798 m

The Southern African Large Telescope (SALT) is closely modeled on the Hobby-Eberly Telescope (HET) concept. The design comprises a spherical primary mirror mosaic of 91 identical 1 m wide hexagons, tilted at a constant zenith distance (37 degrees for SALT), with azimuthal rotation only for target acquisition. The target is then tracked by moving the instrument payload at the primary focus. The payload tracker has a range of ± 6 degrees. The spherical aberration corrector (SAC) provides an F/4.2 beam with an 8 arcminute field of view at prime focus.

1.2 Observing Constraints

SALT is a fixed altitude telescope, and therefore observing with it is more complicated than observing with most ground-based telescopes. SALT can access ~70% of the sky observable at Sutherland, but only during specific "windows of opportunity". Objects are not always accessible by SALT, even though they may be above the horizon. However, the dates an object can be observed during the course of a year are almost identical to that of a more traditional telescope.

Figure 1 shows the region of the sky visible to SALT. This is the annulus on the sky with elevations of 53 ± 6 degrees. The airmass over this elevation range varies from 1.17 to 1.37 with a mean of 1.25. Prominent astronomical objects are marked at their respective declinations.

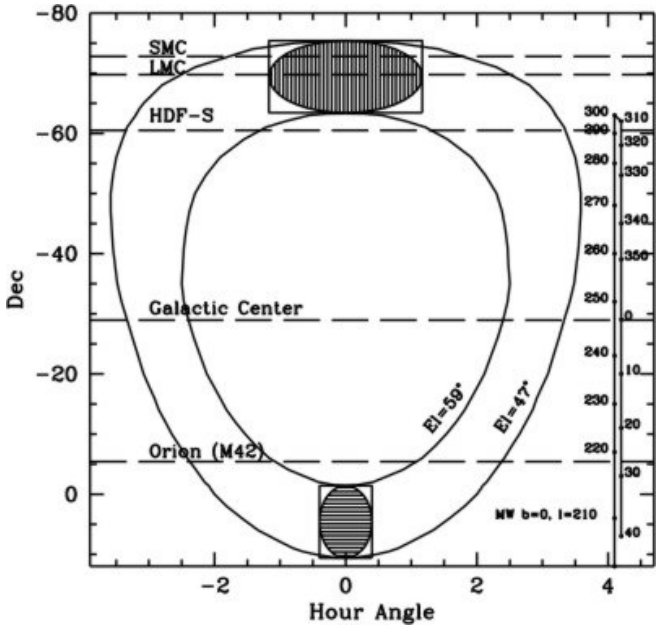

Figure 1. SALT observing annulus as a function of declination and hour angle. The hashed regions show the range of motion for the tracker at two different declinations.

Objects at southerly declinations are visible for longer periods (several hours) compared to those at northerly declinations, where the average time for a single track is only 50 minutes. For all except the most northerly or southerly declinations, objects can potentially be observed twice a night at favorable times of the year.

2 Instrument Overview

2.1 Optical Design

PFIS resides at the prime focus of SALT. The Spherical Aberration Corrector (SAC) delivers a F/4.2 beam providing a flat, 8 arcminute diameter field of view at the focal plane, with a plate scale of 4.5 arcsec/mm.

2.1.1 Collimator and Camera

PFIS is an all-refractive collimator and camera system, optimized for spectroscopic performance in the 320-900 nm wavelength range. The collimator has 9 lenses in 5 groups plus a fold mirror before the last doublet. In the 150 mm diameter collimated beam are the shutter and the dispersers, which include one of six gratings (five volume phase holographic (VPH) gratings and a standard transmitting surface relief grating) or a double-etalon Fabry-Perot system. The camera (F/2.2, 8.6 arcsec/mm) has 9 lenses in 4 groups, with the final lens, a field flattener, being the dewar window. All optical surfaces are spherical except for the first surface in the camera, which is an asphere.

The collimator is designed to work in the 320-1700 nm range, to accomodate a future near-infrared camera. Air-glass interfaces in the collimator will be coated with either a MgF_2 /Solgel hybrid or just a MgF_2 antireflection coating. Camera surfaces will be coated with a MgF_2 /Solgel hybrid or multi-layer antireflection coating.

To compensate for image error introduced by possible differences in filter thicknesses and uncompensated thermal effects, the camera will have an active focus system. Focusing will be accomplished by moving the singlet and the triplet in the camera together. Additionally, the camera will need to be refocused for each configuration, as the imaging was not optimized for all wavelengths simultaneously. However, a fixed focus position can be set for each configuration. Then final focus error due to filters/thermal effects can be removed.

2.1.2 Gratings

PFIS will have a complement of five volume phase holographic (VPH) gratings and one standard surface-relief transmission grating. The gratings were chosen to provide spectroscopic capability over the entire wavelength range of the detector and resolving powers from R=500 to R=5500 (with typical slit widths).

The VPH gratings provide high diffractive efficiency and significantly reduced scattered light as compared to standard surface-relief gratings. Also, VPH gratings can be tuned to shift the diffraction efficiency peak to a desired wavelength. The use of such gratings requires the camera to be able to articulate, to accommodate various grating tilts. The grating will reside on a rotatable stage, and the entire camera will articulate about the same axis as the grating rotation,

so that the grating is always used in a Littrow configuration.

2.1.3 Fabry-Perot Etalons

PFIS will implement a double etalon system, allowing resolving powers from R=500 to R=12500 over a full octave in wavelength (430 - 860 nm). On a telescope the size of SALT, this provides a high dispersion, high spatial resolution diffuse-object capability with a net efficiency that exceeds slit spectroscopy by more than an order of mantidue, since the detector pixels are more efficiently multi-plexed.

The system will have three spectral resolution modes: low (R=500 - 1000, tunable), medium (R=2500), and high (R=12500). Low-resolution mode will use a single etalon, with an interference filter to select the desired interference order (corresponding to wavelength). The medium- and high-resolution modes will use two etalons in series, with the low-resolution etalon and its filter selecting the desired order of the medium- or high-resolution etalon, respectively. Two of the three etalons will be installed at any time; the low-resolution etalon will reside on PFIS at all times, while the one or the other of the medium- and high-resolution etalons will be installed.

2.1.4 Polarimetric Optics

Polarimetric observations will utilize a "wide-field"' design, in which a polarizing beamsplitter in the collimated beam takes the central half of the field and splits it into two orthogonally polarized fields, the "ordinary"' (O) and "extraordinary"' (E) beams. A polarization modulator preceding the beamsplitter modulates the polarization state with time, and the difference between the intensities of the O and E images as a function of time yields the polarization.

The beamsplitter is an array of calcite Wollaston prisms, inserted in the collimated beam just before the first camera element. This ensures that there is no vignetting of the split beam, which would compromise the polarimetric precision. Additionally, by placing the beamsplitter after the dispersers, both the O and E beams have the same wavelength gradient in Fabry-Perot mode.

The modulator consists of two rotating superachromatic mosaic waveplates, a 105 mm half- and a 60 mm quarter-waveplate. The modulator should be ahead of any optical elements with polarization sensitivity, like the fold mirror and the dispersers.

2.2 Detector CCD array

The detector subsystem comprises a cryostat containing a 3x1 mini-mosaic of CCD chips (Figure 2). The chips are E2V (formerly Marconi) 44-82 CCDs (Data Sheet) with 2k × 4k × 15 micron pixels. The mosaic is housed in an evacuated cryostat and thermally connected to the cold end of a Cryotiger, which cools the chips sufficiently to render dark current insignificant while minimizing QE reduction. The detectors are managed by an SDSU III CCD controller, which is in turn controlled by a PC.

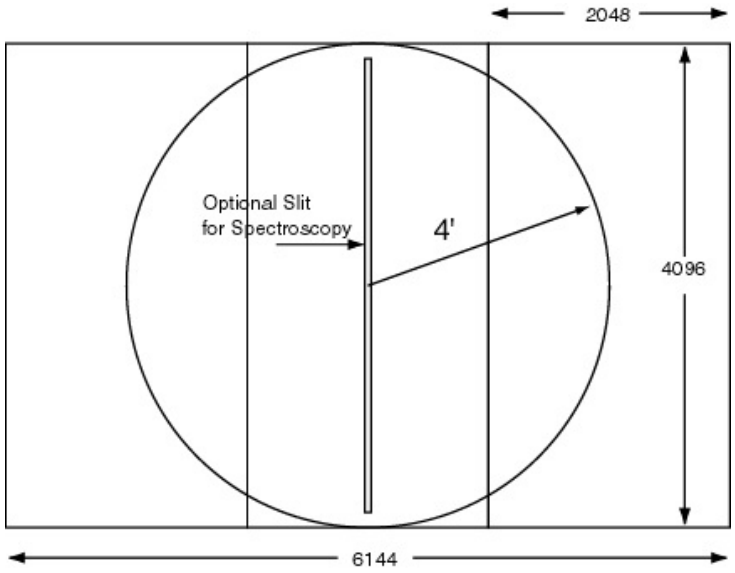

Figure 2. CCD mosaic geometry

2.3 System Efficiency

Figure 3 shows the predicted throughput performance of the PFIS optical system. This plot excludes the CCD QE and any of the dispersers or polarimetric optics. We expect the throughput to be in the 75-82% range across the entire visible camera wavelength range.

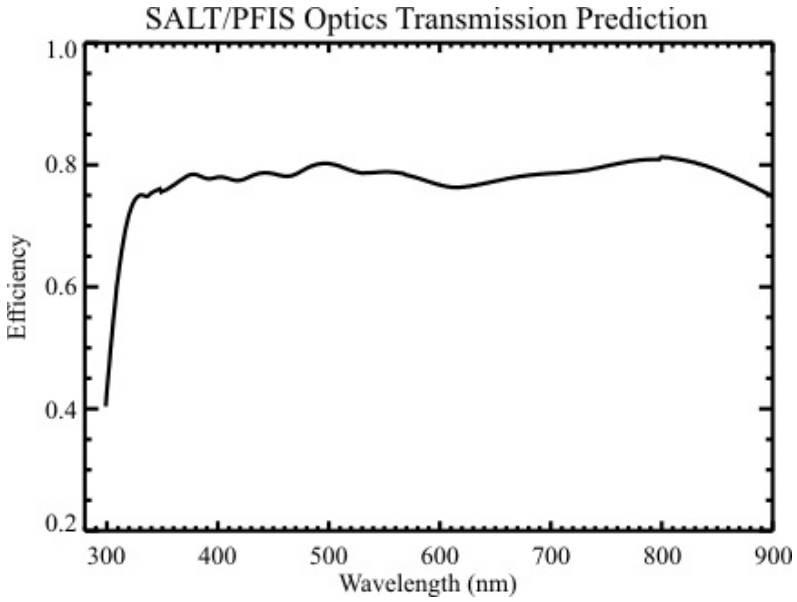

Figure 3. Predicted Throughput

3 Observing Modes

PFIS has three main instrument configurations. These enable three basic observing modes: Imaging, Grating Spectroscopy, and Fabry-Perot Imaging Spectroscopy. Additionally, PFIS employs polarization optics allowing for each of these observing modes to have a polarimetric sub-mode.

3.1 Imaging

The PFIS optical design is not optimized for broad-band imaging. Narrow-band imaging may be performed with either the FP interference filters or possibly additional filters to be added to the complement. However, we expect that SALTICAM will be the primary instrument for SALT imaging programs.

The primary use for PFIS imaging will be for commissioning level astrometric and distortion characterizations. Additionally, PFIS may be used for some context imaging of fields that will be used for multi-slit observations.

More information to come...

3.2 Grating Spectroscopy

PFIS will have a complement of six transmission gratings. One standard surface-relief grating and five volume phase holographic (VPH). VPH gratings have the characteristic that their efficiency varies with input angle, and thus a single grating can cover a large wavelength range with good efficiency by changing the relative angle between the collimated beam and the grating normal, alpha. This is accomplished using a rotating stage. The PFIS camera is then articulated to twice the grating angle since the VPH efficiency curve for a given grating angle typically is at a maximum at the Littrow wavelength (alpha = beta).

Note: All gratings are used in first order only. Second order contamination is removed through the use of order-blocking filters, described below.

Mechanical limitations require that the camera angle be quantized to every 0.75 degrees, with a maximum articulation of 100 degrees. Thus, a finite (but still large) number of camera positions are available. The camera angle determines the central wavelength on the detector, with longer wavelengths associated with larger camera articulation angles.

The angle of the grating also affects spectral resolution. The higher the value of the grating tilt, the higher the spectral resolving power for a given slit width.

Use the VPH grating spectroscopy simulator to determine the optimal grating angle and slit width for your observation.

3.2.1 Grating Complement

Grating	**Wavelength Coverage** (nm)	Usable Angles (degrees)	Bandpass per tilt (nm)	**Resolving Power** (1.25 arcsec slit)
SR300	370-900		390/440	250-600
G0900	320-900	12-20	~300	600-2000
G1300	390-900	19-32	~200	1000-3200
G1800	450-900	28.5-50	150-100	2000-5500
G2300	380-700	30.5-50	100-80	2200-5500
G3000	320-540	32-50	80-60	2200-5500

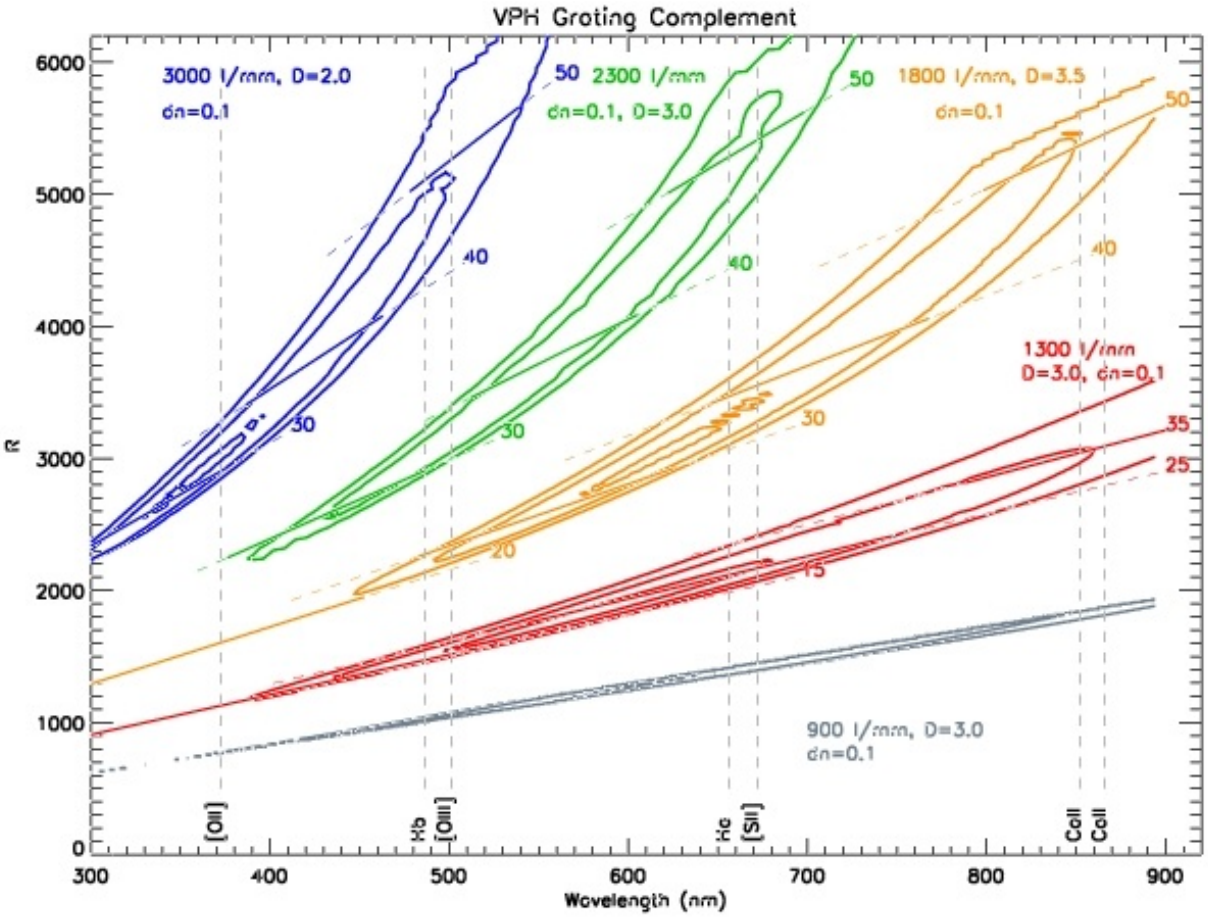

Figure 4. VPH grating efficency vs Resolution and Wavelength

Figure 4 is a contour plot of the VPH grating efficiencies, as calculated using Rigorous Couple Wave (RCW) analysis, in resolving power versus wavelength. The contours correspond to 90%, 70%, and 50%. Wavelength coverage for a few angles is shown for each grating.

3.2.2 Longslit complement

The choice of slit widths is driven by considerations of resolution and throughput. A variety of slits will be available to cover the range of atmospheric seeing conditions expected at the site. For the SALT site, the median seeing is 0.9 arcseconds at the zenith. Seeing varies approximately as

$$FWHM \propto sec(z)^{0.6}$$

For the SALT telescope, where the zenith distance is 37 ± 6 degrees, the factor by which the seeing is degraded from the zenith seeing is 1.14 ± 0.05. Furthermore, the telescope (plus SAC) imaging error budget is 0.6 arcseconds. Therefore, the median spot size at the PFIS focal plane is 1.2 arcsec.

The PFIS slitmask magazine has room for ten tilted longslits. These allow for the SALT Imaging Camera (SALTICAM) to be used as a slitjaw viewing camera. The complement of longslits will include:

* Standard longslits:
    - o 0.60 arcsec wide x 8 arcmin long
    - o 0.90 arcsec wide x 8 arcmin long
    - o 1.20 arcsec wide x 8 arcmin long
    - o 2.00 arcsec wide x 8 arcmin long
* Polarimetric longslits:
    - o 1.20 arcsec wide x 4 arcmin long
* Coronagraphic longslits:
* Nod & Shuffle longslits:
    - o 1.20 arcsec wide x 2.5 arcmin long

Slit Width (arcsec)	**Slit Throughput** for zenith seeing of		
	0.6 arcsec	**0.9 arcsec**	**1.8 arcsec**
0.6	0.561	0.446	0.258
0.9	0.755	0.626	0.379
1.2	0.879	0.764	0.490
2.0	0.990	0.952	0.727

3.2.3 Order-blocking Filters

Five order blocking filters are available, a Clear filter, three UV-blocking filters, UV-32, UV-34 and UV-38 (Figure 5 left), and one blue filter GG455 (Figure 5 right).

3.2.4 Multi-Object Spectroscopy

PFIS will have multi-object spectroscopy capability. Slitmasks will be fabricated using a laser cutting machine and inserted into a magazine that will reside on the insrument. The magazine will carry 30 of these customized slitmasks at any given time. User designed slitmasks will be cut and stored on site and labeled with a bar code for identification.

Peakup holes are cut into the mask and correspond to the focal plane positions of reference stars. Peaking up the position of the slits on the sky requires several images taken at slightly different telescope pointings. The CCD control computer will sum and report the counts within pre-programmed sub-arrays on the chips, and the PFIS computer will command the telescope to the position that produced the highest throughput.

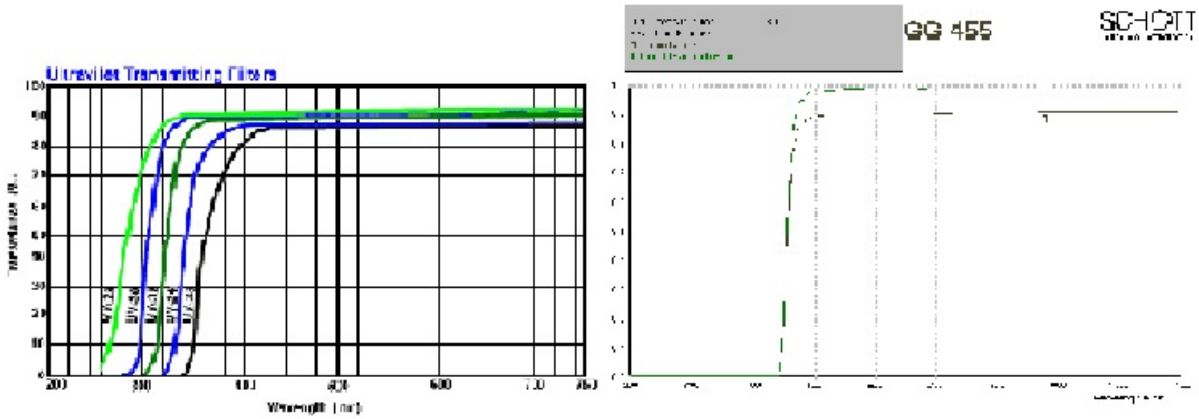

Figure 5. Block Filter transmission curves

One specific characteristic of VPH gratings to keep in mind is that the wavelength dependence of the efficiency depends on the input angle to the grating. In multi-object spectroscopy, the light entering through off-axis (in the dispersion direction) slits will hit the grating at different angles. Thus, the efficiency for the off-axis objects will be different than for the on-axis objects. This will in general not be symmetric either, i.e. objects that are at +2 arcminutes off-axis will have a different wavelength dependence of the efficiency from those at -2 arcminutes off-axis.

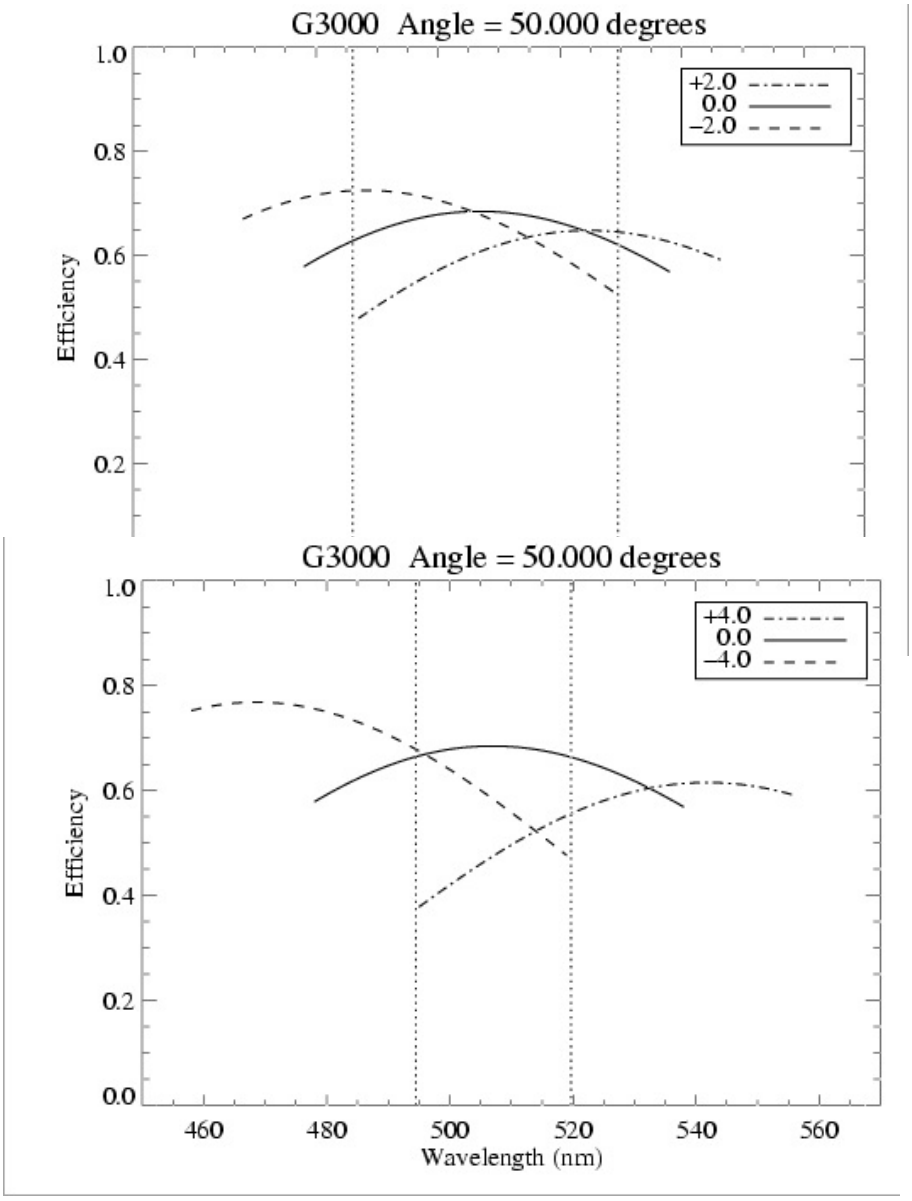

Figure 6/7. Effect of off-axis angle on blaze

Additionally, the wavelength coverage on the detector for off-axis objects will be different than that for on-axis. So, the simultaneous wavelength coverage for a given grating setup with a multi-object slit mask will depend on how far off-axis the objects are.

Figures 6 and 7 demonstrate these effects. They show, for the G3000 grating at 50 degrees grating angle, what the wavelength coverage and efficiency for the on-axis and two off-axis positions is. Note that for the full field (4 arcminutes off-axis) the simultaneous wavelength coverage is reduced and the efficiency can be as much as 50% lower for certain wavelengths.

When contemplating multi-object observations, be sure to use the VPH grating spectroscopy simulator to look at the efficiency curves for the off-axis positions.

3.2.5 Spectropolarimetry

More info to come...

3.3 Fabry-Perot Imaging Spectroscopy

The PFIS Fabry-Perot system provides two-dimensional imaging spectroscopic capabilities. Three spectral resolution modes are provided, each over the wavelength range 430 - 860 nm. The system works with the camera in its imaging configuration (camera angle = zero degrees), the gratings removed, and one or two of the FP etalons inserted into the collimated beam. The full 8 arcmin field of view is imaged onto the detector, with the spectral band selected by the etalons and the appropriate order-selecting filter.

A typical observing sequence consists of taking a series of exposures of an astronomical target, changing the wavelength setting of the FP system for each exposure to cover the relevant spectral range about a spectral feature of interest. Atmospheric transparency is monitored during each exposure by the guider. Wavelength zero-point calibration exposures of a standard spectral lamp are taken before and afer the sequence. Flat-field and full wavelength calibration sequences are run during daylight hours.

3.3.1 Etalons

The FP system uses servo-controlled etalons manufactured by ICOS. Piezoelectric positioners set the parallelism and the gap of the etalon plates, and the plate positions are monitored by capacitance sensing.

The spectral resolution of an etalon is set by the size of the spacing between its plates and by their reflectivity; this resolution is fixed for a given etalon (although the lowest resolution etalons have small enough gaps that they can be tuned by their piezos through approximately a factor of two in resolving power). The system has four spectral resolution modes: tunable filter (TF), low (LR), medium (MR), and high (HR). Tunable filter and low-resolution modes use a single etalon, with an interference filter to select the desired interference order (corresponding to wavelength). The medium- and high-resolution modes use two etalons in series, with the low-resolution etalon and its filter selecting the desired order of the medium- or high-resolution etalon, respectively.

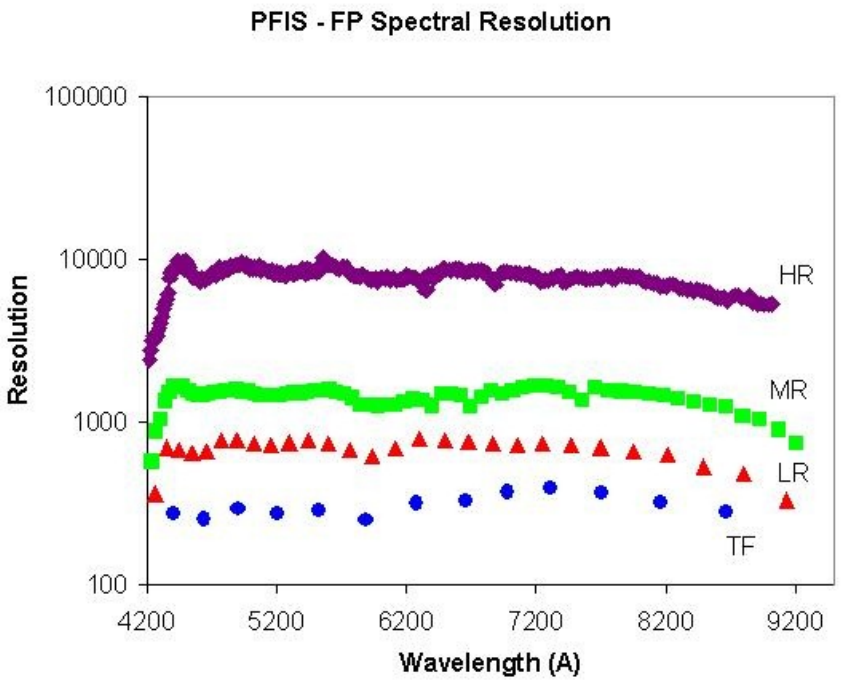

Figure 8. Fabry-Perot Spectral resolution vs wavelength

Be aware of the standard spectroscopist's rule of thumb: with reasonable signal-to-noise, you can measure a velocity accurate to about 1/20 the FWHM of the line profile. For example, in measuring galaxy rotation curves, you are probably interested in a precision of about 5 to 10 km/sec; that suggests a resolution of about 1500, or MR mode. If, on the other hand, you are investigating line profile shapes, you obviously need higher resolution. Don't over-resolve! The cost in total observing time varies as the square of the resolution

Approximately 30 interference filters (of resolving power R=50) will be required to isolate the FP orders over the entire spectral range. Only 15 will be installed in the magazine at any one time, so the operating queue will be structured to limit the number of filters needed on a given night.

The wavelength of a single FP image is not constant over the field, but varies quadratically with distance from the optical axis. The field of view at approximately constant wavelength (the so-called "bull's-eye") is 1.3' × $(10450 / R)^{1/2}$, set by the focal length of the PFIS collimator. The total wavelength variation from the optical axis to the edge of the field of view is 0.9969 x the central wavelength (2.1 nm at 656.3 nm).

3.3.2 Efficiency

For a continuum object of magnitude B=V=R=I=20, the table below lists the expected detected photon rate per second in each FP resolution bandpass, and the corresponding sky rate

(photons/sec) per square arc second at new moon. Binning 2×2 or 4×4 gives 0.25" or 0.5" pixels respectively, and the read noise is about 3 e^- per pixel. For emission lines, a typical HII region has a luminosity of 10^{38} erg/sec, so at a distance of 10 Mpc it will give about 440 detected Ha photons/sec and subtend ~1"; the diffuse Hα background in galaxies is typically 10 - 100× fainter.

Table : Detected photon fluxes (counts/second) for continuum objects

Wavelength	**TF**		**LR**		**MR**		**HR**	
(nm)	**m=20**	**sky**	**m=20**	**sky**	**m=20**	**sky**	**m=20**	**sky**
450	28.6	2.88	11.8	1.19	2.8	0.28	0.54	0.054
550	27.2	6.84	10.0	2.52	3.0	0.69	0.56	0.14
650	21.4	10.2	8.9	4.23	2.9	1.25	0.58	0.26
800	17.4	18.9	9.5	8.17	2.9	3.23	0.60	0.65

3.3.3 Filters

There are forty narrow-band intereference filters that cover the entire spectral range of the Fabry-Perot system:

Table : Fabry-Perot Filters (as of 2005 July 8)

Filter #	Design (Ang)		Revised (Ang)		As Built (Ang)		Trans (%)
	Center	FWHM	Center	FWHM	Center	FWHM	
1	4340	80			4349.4	79.1	71.7
2	4400	85	4412.3	92.4			
3	4465	90			4478.1	84.9	80.9
4	4530	90					
5	4600	95					
6	4670	100					
7	4740	100			4760.2	111.1	82
8	4820	105					
9	4895	110			4912.5	105	81.3
10	4975	110	4990.6	107.5			
11	5060	115			5071.5	110.5	86.4
12	5145	120	5152.1	109.2			

Filter #	Design (Ang)		Revised (Ang)		As Built (Ang)		Trans (%)
	Center	FWHM	Center	FWHM	Center	FWHM	
13	5235	120			5237	119.1	85
14	5325	125					
15	5420	130					
16	5520	135					
17	5620	140			5631.5	137	90
18	5725	145	5731.1	133.6			
19	5830	145			5833.6	142.8	87.3
20	5945	150	5946.5	164.1			
21	6055	155			6062.2	148.6	89.4
22	6170	155	6178.8	169			
23	6290	160			6300.2	158.3	80.7
24	6410	160	6418.4	161.5			
25	6530	160			6535.5	156	88.4
26	6645	160	6647.4	148.8			
27	6765	160			6765	167.5	86.2
28	6885	160	6894.3	181.8			
29	7005	165			7020.8	162.1	81
30	7130	170	7131.3	140.4			
31	7260	180			7252.7	184.1	80.9
32	7390	190	7400	218			
33	7535	200			7555.6	200.8	82
34	7685	210	7691.9	168.9			
35	7840	215			7831.6	207.6	81.8
36	8005	225	7999	249.2			
37	8175	235			8175.1	225.2	78.2
38	8350	245					
39	8535	260					
40	8730	275					

3.4 Polarimetry

The polarization optics employ a "wide-field" design, in which a polarizing beamsplitter in the collimated beam takes the central half of the field and splits it into two orthogonally polarized fields, the "ordinary" (O) and "extraordinary" (E) beams. One (or two) waveplates can be inserted into the beam, right after the field lens in the collimator, and will modulate the polarization state with time. The difference between the intensities of the O and E images as a function of time

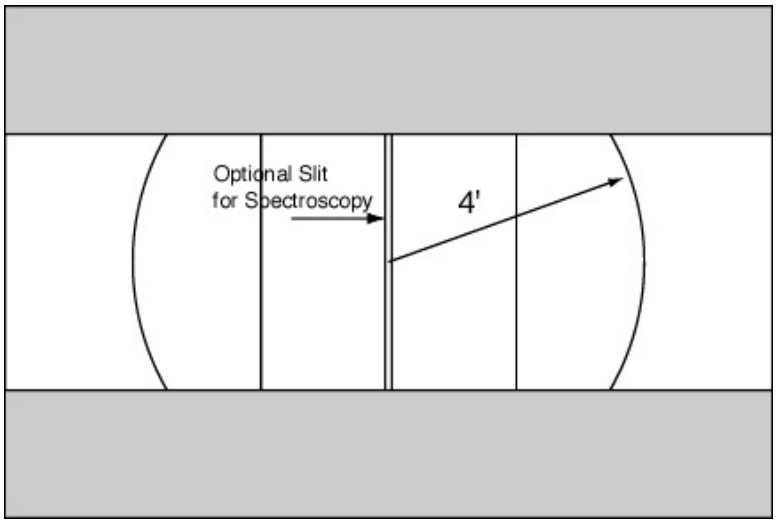

Figure 9. Mask Geometry for Polarimetry

yields the polarization.

For the polarimetric modes, only the central 4 arcminute portion of the focal plane is used (accomplished using a short slit for spectroscopy or a special mask blocking the upper and lower quarter of the field of view for imaging - see Figure 9). Frame transfer operations are not possible with polarimetry, because the E and O beams use up space on both sides of the frame transfer boundary.

3.4.1 Waveplate Modes

The waveplate modulators are to be used in three modes, linear, circular, and "all-Stokes". For ease of operation, the waveplates are in the same order in all modes, half-wave first. Table 1 gives the waveplate angle progression for each mode. The angle shown is that between the waveplate optic axis and the beam-splitter polarization axis, which is perpendicular to the dispersion direction.

Linear		Circular		All Stokes	
1/2 wave	1/4 wave	1/2 wave	1/4 wave	1/2 wave	1/4 wave
0	-	0	45	0	0
45	-	0	-45	22.5	33.75
22.5	-	22.5	-45	45	67.5
67.5	-	22.5	45	67.5	101.25
11.25	-	45	45	90	135
56.25	-	45	-45	112.5	168.75

33.75	-	67.5	-45	135	202.5
78.75	-	67.5	45	157.5	236.25

3.4.2 Efficiency

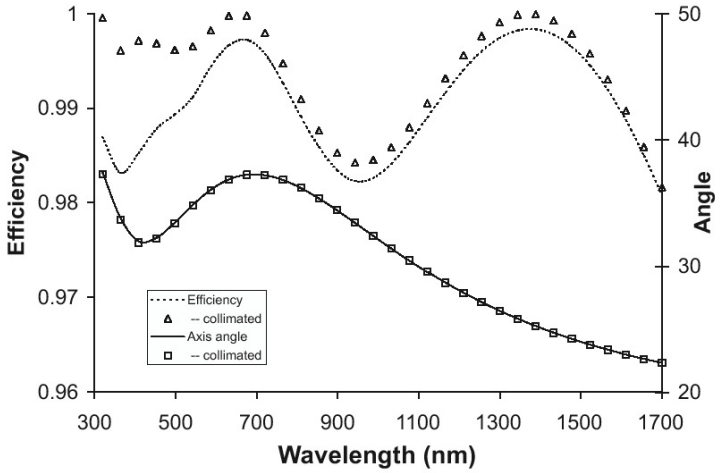

Figure 10. Halfwave Plate Axis and Polarization

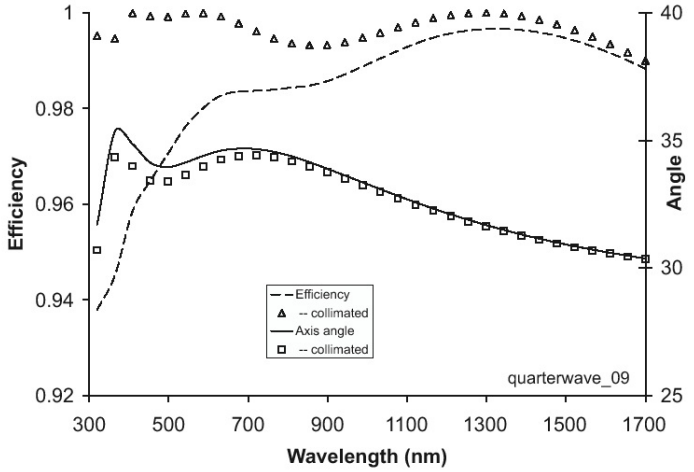

Figure 11. Quarterwave Plate Axis and Polarization Efficiency

4. Detector Subsystem

4.1 CCD QE

Figure 12 is a plot of the measured quantum efficiencies of the CCDs as delivered by E2V. SALT-03 will be used at the blue end of the array and SALT-06 at the red end.

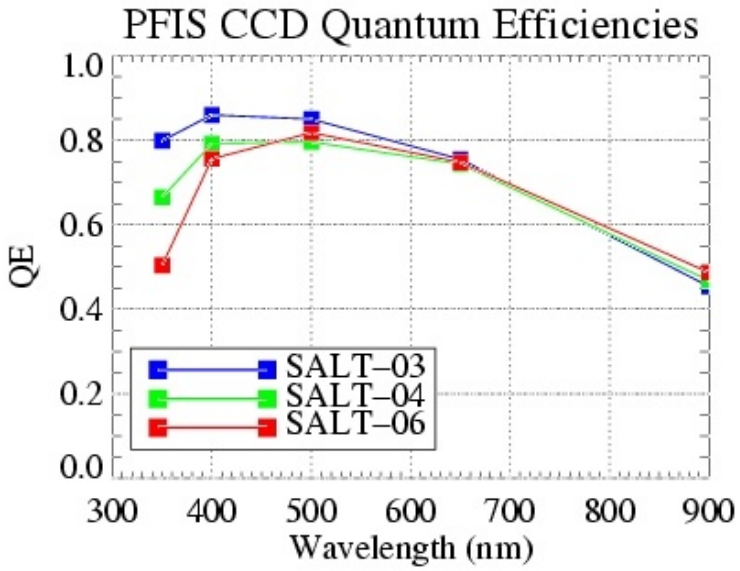

Figure 12. CCD mosaic QE's

4.2 Readout Modes

4.2.1 Normal Readouts

This is the standard mode for operating CCD cameras involving shuttered operation. It is assumed that 1×1 prebinning will never be used and that the minimum prebinning will be 1×2 prebinning (high resolution spectroscopy) or 2×2 prebinning (all the rest).

Detector subsystem operations will include:

* Clearing the detector prior to readout in: 0.205 sec

* Shutter opening in: 0.150 sec

* Exposure

* Shutter closing in: 0.150 sec

* Readout of the detector in: 22.201 sec (1x2 prebinning, 3 e-/pix readout noise)

OR

* Readout of the detector in: 11.203 sec (2x2 prebinning, 3 e-/pix readout noise)

Faster readout is possible (by about a factor 3) with 5 e-/pix readout noise.

4.2.2 High Time Resolution Readouts

It is assumed that 1x1 prebinning will never be used and that the minimum prebinning will be 1×2 prebinning (high resolution spectroscopy) or 2×2 prebinning (all the rest). Frame transfer operation is required to enable a continuous sequence of exposures, frame transfers and readouts (while the next exposure is accumulating). The shutter will be open throughout the sequence.

Detector subsystem operations will include:

* Shutter opening (time irrelevant)

* Clearing the detector prior to the first exposure in: 0.205 sec

* Exposure

* Frame transfer in: 0.102 sec

* Vertical operations during readout: 0.103 sec

* Readout of the detector in: 10.998 sec (1x2 prebinning, 3 e-/pix readout noise)

OR

* Readout of the detector in: 5.499 sec (2x2 prebinning, 3 e-/pix readout noise)

OR

* Readout of the detector in: 3.190 sec (1x2 prebinning, 5 e-/pix readout noise)

OR

* Readout of the detector in: 1.595 sec (2x2 prebinning, 5 e-/pix readout noise)

with repetitions of frame transfer and readout for as long as desired. The minimum exposure time should be a little longer than the above readout times (say 0.2 sec: TBC2) to ensure that the next readout does not begin before the data are read out, displayed (if necessary) and stored. Minimum total cycle times of about 11.5, 6.0, 3.5 and 2.0 sec (assuming a 0.2 sec safety margin) would be realized for the parameters shown. Note that the image is smeared during the 0.102 sec needed for frame transfer.

The above readout times assume that the image is formed in the image section half of the chip, which extends 4 arcmin from the frame transfer boundary in the cross dispersion direction and away from the readout register. If a slit plane mask is used to limit (window) the imaging area to less than 4 arcmin, significantly higher time resolution can be gained with frame transfer operation. In such an arrangement, a frame transfer does not take place at the end of an exposure; instead, only the imaged area is transferred across the frame transfer boundary to save on row transfer time (50 msec/row). The following table shows transfer times, vertical transfers during readout and readout times as a function of imaged area for 2x2 prebinning and 5 e-/pix readout noise (2.9 msec/pix readout rate).

The first row is a repetition of the information given previously. The minimum exposure times should be significantly longer than these readout times in order to avoid too much degradation by image smearing during the row transfers.

Overheads such as associated with data storage within the host PC may play a significant role in the fastest applications so that the above performance needs verification (TBC3).

Image Height (arcseconds)	Image Height (Pixels)	Transfer Time (seconds)	Store Transfer Time (seconds)	Readout Time (seconds)
4	2048	0.102	0.102	1.595
2	1024	0.051	0.051	0.797
0.5	256	0.013	0.013	0.199
0.125	64	0.003	0.003	0.05

4.2.3 Charge Shuffling

This is not strictly readout; instead, it involves shuffling the charge vertically in either direction. Each vertical transfer takes 50 msec/row. The Detector subsystem will be supplied with the direction and number of row operations required and will execute the sequence (starting after some time still to be specified?).

4.2.4 Drift Scanning

This will require the rows of the detector to be clocked at a tunable rate (from 30 to 118 rows/sec), and the readout register to be readout in a time much shorter than this vertical clock rate.

Detector subsystem operations will include:

* Clearing the detector in: 0.205 sec

* Shutter opening (time irrelevant)

* Performing one vertical transfer every 8.475 - 33.333 millisec (a function of target declination). The time needed for the vertical transfer is 0.050 millisec

* Readout register readout in: 5.37 millisec (2 pix prebinning, 3 e-/pix readout noise) (unprebinned slow readout is too slow for the vertical transfer repeat time)

OR

* Readout register readout in: 3.12 millisec (no prebinning, 5 e-/pix readout noise)

OR

* Readout register readout in: 1.56 millisec (2 pix prebinning, 5 e-/pix readout noise).

with repetitions of vertical transfers and readout register readouts for as long as desired.

List of TBCs

TBC1 - Readout rates and associated readout noise

TBC2 - Exposure time overhead to ensure readout is complete before the next frame transfer operation

TBC3 - Performance in subsecond exposures needs to be verified

Appendix A. Technical Information

A.1 PFIS Papers

"The Prime Focus Imaging Spectrograph for the Southern African Large Telescope: optical design."

Burgh, E. B., Nordsieck, K. H., Kobulnicky, H. A., Williams, T. B., O'Donoghue, D., Smith, M. P., Percival, J. W. 2002, /Proceedings of SPIE/, Vol. 4841, 1463.

"The Prime Focus Imaging Spectrograph for the Southern African Large Telescope: operational modes."

Kobulnicky, H. A., Nordsieck, K. H., Burgh, E. B., Smith, M. P., Percival, J. W., Williams, T. B., O'Donoghue, D. 2002, /Proceedings of SPIE/, Vol. 4841, 1634.

"Instrumentation for high resolution spectropolarimetry in the visible and far-ultraviolet."

Nordsieck, K. H., Jaehnig, K. P., Burgh, E. B., Kobulnicky, H. A., Percival, J. W., Smith, M. P. 2002, /Proceedings of SPIE/, Vol. 4843, 170.